

# Determining CO<sub>2</sub> consumption from elemental change in soil profiles developed on carbonate and silicate rocks

Daojing Li · Hongbing Ji

Received: 10 September 2014 / Revised: 4 November 2014 / Accepted: 11 November 2014 / Published online: 7 February 2015  
© Science Press, Institute of Geochemistry, CAS and Springer-Verlag Berlin Heidelberg 2015

**Abstract** To further understand the roles of carbonate and silicate rocks in regulating the atmosphere/soil CO<sub>2</sub> level, the flux of CO<sub>2</sub> consumed by the chemical weathering of silicate and carbonate rocks was determined from the elemental change in soil profiles. Results showed that the chemical weathering of carbonate rocks mainly occurred at the rock-regolith interface, and that the further weathering of the residua soil on the carbonate rocks was similar to that of the granite profile. Chemical weathering of the silicate rocks occurred through the whole profiles. Therefore, CO<sub>2</sub> consumed per volume by the silicate profiles [ $M_{sr}$  (CO<sub>2</sub>)] and the residues on carbonate rocks [ $M_{cr}$  (CO<sub>2</sub>)] were calculated based on the elemental weathering gradients. CO<sub>2</sub> consumed by carbonate protolith [ $M_{cp}$ (CO<sub>2</sub>)] was calculated from the elemental change at the rock-regolith interface. The  $M_{sr}$  (CO<sub>2</sub>) were about tens to thousands orders of magnitude greater than  $M_{cr}$  (CO<sub>2</sub>). Even so, this demonstrated that the residues on carbonate rocks could be a sink of CO<sub>2</sub> on long-term scales. The  $M_{cp}$  (CO<sub>2</sub>) was about four times larger than  $M_{sr}$  (CO<sub>2</sub>), which demonstrated that carbonate rocks played a more important role in regulating the CO<sub>2</sub> level than the silicate rocks did during the pedogenic process of the profiles.

**Keywords** Carbonate rocks · Silicate rocks · CO<sub>2</sub> consumption · Soil profiles

## 1 Introduction

Chemical weathering of silicate and carbonate rocks is an important source of control on the regulation of the level of atmospheric CO<sub>2</sub>, and thereby exerts control on global climate variations (Hartmann et al. 2009; Moosdorf et al. 2011; Moquet et al. 2011). To improve our understanding of that control, many studies about carbonate and silicate weathering have been carried out (Nesbitt and Young 1982; Suchet and Probst 1995; Macpherson et al. 2008; Li et al. 2010; Heckman and Rasmussen 2011; Moosdorf et al. 2011; Zeng et al. 2012). Silicate weathering studies are conducted through relatively input–output calculations, from changes in solute compositions in pore water or ground water, or from the elemental differences between protolith and the weathered regolith (Kenoyer and Bowser 1992; White et al. 1996; Murphy et al. 1998; White 2002; White et al. 2005b). Chemical weathering of silicate minerals has been proposed to be a sink of atmospheric CO<sub>2</sub> on the geological time scale (Ridgwell and Zeebe 2005). Carbonate minerals are more reactive and soluble than silicate minerals and thus regulate the geochemistry of surface waters (Horton et al. 1999; White et al. 2005a). Therefore, most studies about carbonate weathering are confined in the study of HCO<sub>3</sub><sup>−</sup> ions in the surface water in carbonate watersheds (Macpherson et al. 2008; Li et al. 2010; Zeng et al. 2012). Few approaches have been taken on the soil profiles developed on carbonate rocks. Chemical weathering of carbonate minerals has been proposed to consume atmospheric CO<sub>2</sub> on a relatively short-term scale but not produce a net carbon sink on a long-term scale, because the CO<sub>2</sub> consumed by carbonate minerals would get back to the atmosphere due to

D. Li (✉) · H. Ji  
State Key Laboratory of Environmental Geochemistry, Institute of Geochemistry, Chinese Academy of Sciences,  
Guangzhou 550002, China  
e-mail: lidaojing45@163.com

H. Ji  
College of Resource Environment and Tourism, Capital Normal University, Beijing 10048, China  
e-mail: jih\_0000@126.com

the formation of marine carbonate sediments (Berner et al. 1983; Berner 1991, 1997; Goudie and Viles 2012). Our previous work demonstrated that the weathering of carbonate rocks includes the weathering of carbonate minerals and the insoluble residues (Ji et al. 2004a, b). The weathering process of the residue soils, which is similar to the weathering of non-carbonate rocks, may produce a net carbon sink. This contradicted the previous belief that carbonate rocks did not produce a carbon sink on a long-term scale. This paper presents a systematic methodology for calculating CO<sub>2</sub> consumption by the weathering of carbonate and silicate rocks based on elemental changes in soil profiles, in order to further understand the roles of carbonate and silicate rocks in regulating atmospheric CO<sub>2</sub>.

## 2 Materials and methods

### 2.1 Site description

The study of soil profiles consisted of four profiles developed on carbonate rocks and two profiles developed on silicate rocks. The carbonate profiles are located in the Guizhou Province, including those at Puchang of Suiyang County (PC), Xinpu town in Zunyi (XP), Pingba County (PB) and Hezhang County (HZB). One silicate profile is at

Hezhang County (HZX) and the other is at Gunbei village (GB) in Rongshui County, which is in the northern Guangxi Province bordering the Guizhou Province (Fig. 1). The sampling sites are all in hilly areas. The climate of the study area was during the transition zone between the East Asian and the South Asian monsoons. As the elevation increased from the east to the west, the temperature and precipitation decreased. The six profiles were selected because they were distributed from the east to the west (Fig. 1) and were developed on different kinds of rocks (Table 1), based on which the effects of climate and underlying materials on weathering has been discussed. Detailed geographical and climate information of each site is tabulated in Table 1.

### 2.2 Sampling and analyzing methods

The soil profiles were obtained by digging from the bottom to the top and were classified by soil color, texture, major element content, and soil horizon characteristics (Table 1). The profiles can be divided into three horizons: the soil horizon (A-horizon, top for farming layer), the regolith horizon (B-horizon, weathered layer) and the weathering bedrock horizon (C horizon), which can be then subdivided into the flour layer (C1-horizon), the cracked rock layer (C2-horizon) and the parent rock layer (C3-horizon). The “regolith” mentioned below refers to both the B and A

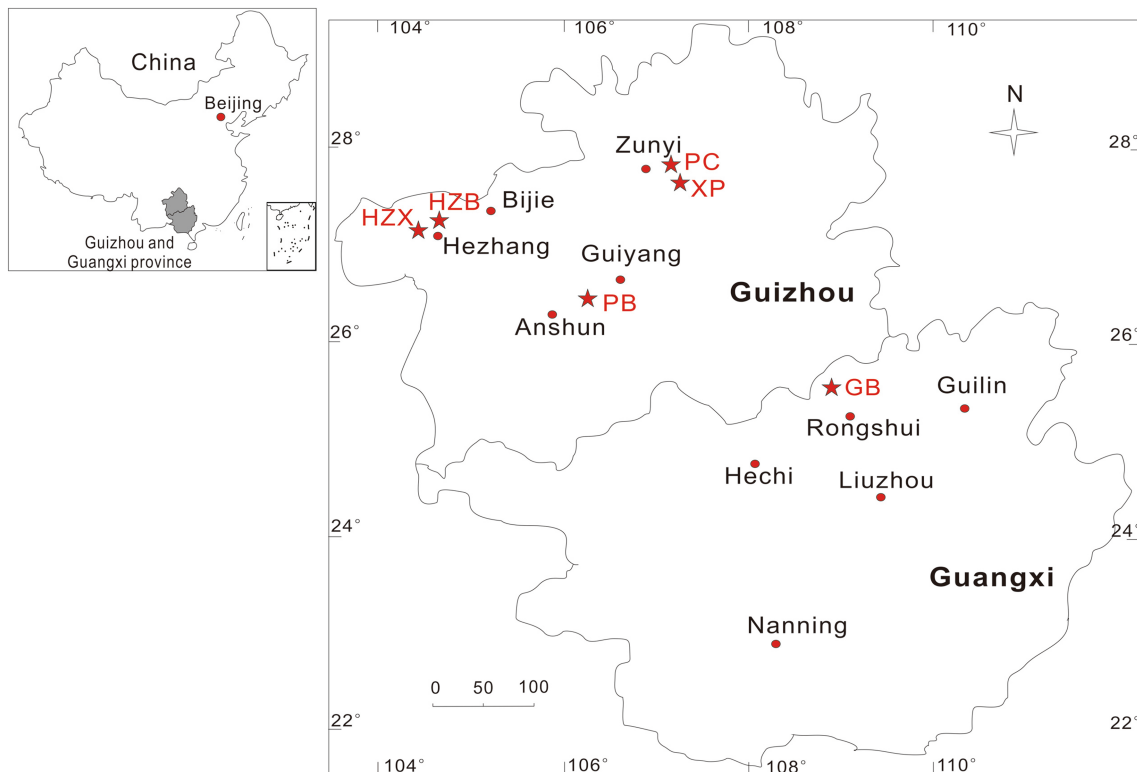


**Fig. 1** Location of study sites in Guizhou and Guangxi Province. Red pentagram indicates the locations where the soil profiles were sampled. Red dots indicate the main cities

**Table 1** Geomorphological and climatic information of the soil profile

Profile name	Type of soil (Chinese/US/FAO)	Longitude	Latitude	Type of bedrock	Elevation (m)	Mean annual temperature (°C)	Mean monthly temperature of the warmest month (°C)	Mean monthly temperature of the coldest month (°C)	Mean annual precipitation (mm/year)	Rainy seasons	Proportion of summer half year precipitation in annual precipitation (%)
PC	Cambisols/Inceptisols/Cambisols	107°02'	27°51'	T <sub>1</sub> y	951	15	22	1	1,160	April to October	76.8
XP	Argosols/Alfisols/Acrisol	107°03'	27°44'	C <sub>2,3</sub> ls	853	13	26	5	1,160	April to October	76.8
PB	Ferralsols/Oxisols/Ferralsols	106°21'	26°25'	T <sub>1</sub> a	1,256	18	24	6	1,298	April to October	78.9
HZB	Argosols/Alfisols/Acrisol	104°43'	27°08'	P <sub>1</sub> m	1,689	12	34	-3	927	May to September	81.8
HZX	Argosols/Alfisols/Acrisol	104°39'	27°08'	P <sub>2</sub> B	1,681	12	34	-3	927	May to September	81.8
GB	Cambisols/Inceptisols/Cambisols	108°52'	25°21'	γ <sub>2</sub>	718	19	37	7	1,803	March to August	77.2

T<sub>1</sub>y early mesozoic–triassic limestone, C<sub>2,3</sub>ls upper–middle Cambrian dolomites, T<sub>1</sub>a early–middle Triassic dolomites, P<sub>1</sub>m lower Permian limestone, P<sub>2</sub>B upper–Permian basalt, γ<sub>2</sub> mesoproterozoic granite

horizons unless otherwise specified. Not all the profiles consist of all the horizons (Table 2). Parent rock samples that were too deep to dig were collected from cores nearby. The soils were collected using a hand hammer and a small shovel, and were sampled at different intervals, depending on profile depth and soil properties. When a distinct change appeared in the soil color or texture, they were not sampled at intervals, but the soil with the different characteristics were removed. A soil sample of 5 cm in vertical width was randomly collected from each horizon. A geological map of the Guizhou Province and Guangxi Province was used to identify the parent material in the field. Each parent rock sample was identified by its texture, structure, shape and color, from at least three rock fragments.

Soil samples were dried in the oven at 45 °C for 2 days, with parts of each being ground to pass a sieve (mesh 200) for further analysis. The bulk density of the regolith samples was determined with the cutting-ring method, referring to the GB/T 50123-1999. The bulk density of the rock was determined with the paraffin method (GB/T 50123-1999). The major oxides of the rock and regolith samples were analyzed by X-ray fluorescence spectrography (XRF) by using the Philips PW2404 X-ray fluorescence spectrometer and referring to the GB/T 14506.14-2010 and GB/T 14506.28-2010. The trace and rare earth element concentrations were measured using Inductively Coupled Plasma Mass Spectroscopy (HR-ICP-MS) (Element I, Finnigan MAT Company). The mineral composition of the carbonate rocks was analyzed using X-ray diffraction (XRD). The mineral composition of the silicate rocks was calculated according to the CIPW norm mineral calculation method based on major oxides.

### 3 Results

The vertical distributions of major oxides, trace elements, chemical index of alteration (CIA) (Nesbitt and Young 1982) and the loss on ignition (LOI) are listed in Table 2. The CIA is used to estimate the weathering intensity of the regolith. An obvious increase occurs at the interface between the C horizon and B horizon for each site (Table 2). The LOI is extremely high for parent carbonate rocks, reflecting a high carbonate content. High LOI in the regolith samples may reflect the influence of high water-bearing phases (mainly clay minerals) and organic matter (Ji et al. 2004a).

An Al<sub>2</sub>O<sub>3</sub>–CaO\* + Na<sub>2</sub>O–K<sub>2</sub>O (A–CN–K) ternary diagram was drawn based on the major oxides content (where CaO\* represents Ca in the silicate fraction) (Fig. 2). In the A–CN–K ternary diagram, there are two weathering trends, one parallel to the A–CN side (weathering trend 1), and the other parallel to the A–K side (weathering trend 2) (Fig. 2). Weathering trend 1 represents the process of leaching Ca

**Table 2** The vertical distributions of major oxides, trace elements, chemical index of alteration (CIA) and loss on ignition (LOI)

Horizon	Depth (m)	SiO <sub>2</sub> (wt%)	Al <sub>2</sub> O <sub>3</sub> (wt%)	Fe <sub>2</sub> O <sub>3</sub> (wt%)	MgO (wt%)	CaO (wt%)	Na <sub>2</sub> O (wt%)	K <sub>2</sub> O (wt%)	MnO (wt%)	TiO <sub>2</sub> (wt%)	P <sub>2</sub> O <sub>5</sub> (wt%)	Sr (μg g <sup>-1</sup> )	Rb (μg g <sup>-1</sup> )	Ba (μg g <sup>-1</sup> )	CIA <sup>a</sup>	LOI (%)		
PC																		
A	0.00	51.16	15.40	11.81	3.98	1.59	0.67	0.29	2.05	0.16	2.61	0.24	64.40	88.30	239.00	346.00	82.90	13.92
	0.10	60.72	13.39	10.66	0.99	0.90	0.33	0.18	1.56	0.19	2.85	0.10	46.40	82.70	242.00	344.00	85.40	8.99
B	0.30	60.37	13.24	11.38	0.56	0.82	0.28	0.12	1.40	0.21	2.87	0.10	42.40	78.90	197.00	356.00	87.30	9.05
	0.50	59.83	13.53	11.68	0.63	0.81	0.28	0.10	1.36	0.18	2.80	0.09	41.50	77.70	189.00	342.00	88.30	9.26
	0.70	59.89	14.24	10.66	0.67	0.98	0.30	0.17	1.83	0.15	2.38	0.10	42.90	88.50	200.00	313.00	84.90	9.20
	0.90	55.66	16.68	11.06	0.26	1.20	0.32	0.12	2.23	0.13	2.21	0.13	40.10	102.00	176.00	311.00	85.60	10.10
	1.10	61.14	13.38	10.89	0.22	0.87	0.30	0.10	1.43	0.12	2.12	0.10	39.20	77.40	144.00	277.00	87.70	9.14
	1.30	61.31	13.46	10.75	0.34	0.86	0.30	0.11	1.37	0.13	2.43	0.10	40.10	76.30	155.00	305.00	87.90	9.07
	1.50	61.39	13.88	10.49	0.22	0.91	0.30	0.10	1.49	0.12	2.20	0.10	37.70	78.30	153.00	292.00	87.60	8.89
	1.70	64.39	13.29	9.37	<0.10	1.07	0.28	0.09	1.81	0.13	1.25	0.11	35.00	76.30	101.00	208.00	85.50	8.11
	1.90	59.45	15.43	10.25	0.18	1.19	0.34	0.09	1.90	0.17	1.55	0.12	34.60	89.00	128.00	239.00	86.70	9.41
	2.10	70.88	11.85	6.17	0.17	1.17	0.27	0.07	2.05	0.14	0.72	0.10	28.20	70.50	70.80	233.00	82.90	6.44
C2	2.20	98.14	0.55	0.28	0.15	0.08	0.14	0.05	0.07	0.01	0.04	0.01	51.20	2.21	13.00	6.52	68.10	0.63
C3	nd	12.58	0.61	0.40	0.29	0.74	0.69	0.21	0.06	0.03	0.09	0.02	1,220.00	1.71	5.78	8.31	45.00	37.76
XP																		
A	0.00	63.07	13.12	7.03	2.20	0.91	0.33	0.11	1.25	0.07	1.20	0.08	52.70	75.00	199.00	367.00	88.50	12.82
	0.05	67.97	11.26	5.85	2.11	0.84	0.43	0.12	1.27	0.07	1.31	0.07	51.50	68.80	213.00	397.00	86.40	10.76
	0.10	70.06	11.59	6.12	0.91	0.84	0.30	0.12	1.31	0.07	1.35	0.06	53.10	67.90	222.00	384.00	86.40	7.97
	0.20	73.47	10.24	5.10	0.75	0.70	0.26	0.11	1.10	0.06	1.42	0.06	56.20	63.30	203.00	435.00	86.70	7.27
B	0.30	60.07	16.96	8.09	0.49	1.12	0.26	0.11	1.49	0.03	1.21	0.05	55.00	88.30	206.00	303.00	89.50	10.49
	0.40	54.49	19.80	9.18	0.41	1.28	0.28	0.10	1.64	0.03	1.11	0.05	56.30	103.00	220.00	246.00	90.30	11.93
	0.50	56.02	18.79	8.80	0.54	1.25	0.28	0.11	1.69	0.03	1.14	0.06	57.80	100.00	225.00	269.00	89.60	11.51
	0.60	54.96	19.51	8.86	0.63	1.31	0.27	0.10	1.89	0.04	1.11	0.06	58.10	107.00	247.00	261.00	89.10	11.86
	0.70	54.38	19.80	9.00	0.54	1.34	0.28	0.10	2.01	0.06	1.10	0.06	57.80	103.00	247.00	241.00	88.70	11.76
	0.80	53.20	20.30	9.20	0.55	1.40	0.27	0.10	2.04	0.06	1.07	0.05	60.40	109.00	267.00	239.00	88.90	12.16
	0.90	55.15	19.56	8.90	0.74	1.33	0.29	0.11	2.02	0.06	1.03	0.06	59.40	107.00	263.00	222.00	88.40	11.32
	1.00	53.65	19.92	9.02	0.50	1.33	0.29	0.11	2.03	0.06	1.04	0.06	60.20	110.00	281.00	223.00	88.60	11.91
	1.10	52.29	20.79	9.46	0.53	1.43	0.33	0.12	2.02	0.06	1.04	0.06	63.30	114.00	274.00	224.00	89.00	12.35
	1.20	48.14	22.58	10.19	0.56	1.64	0.38	0.11	2.15	0.06	0.97	0.06	68.90	123.00	291.00	205.00	89.40	13.65
	1.30	45.14	23.67	10.77	1.01	1.76	0.49	0.11	2.07	0.07	0.91	0.08	62.30	124.00	284.00	190.00	90.10	14.89
C1	1.40	8.02	2.98	1.48	0.15	18.84	26.29	0.03	0.42	0.02	0.16	0.02	48.50	16.20	44.40	2.40	84.30	46.24
C2	1.50	0.77	0.24	0.19	0.32	21.46	30.36	0.02	0.08	0.01	0.02	0.01	50.70	1.50	5.63	30.40	60.30	41.83
C3	nd	1.34	0.22	0.17	0.14	21.35	30.07	0.02	0.14	0.01	0.02	0.01	64.10	1.24	31.60	1.70	50.30	46.08

Table 2 continued

Horizon	Depth (m)	SiO <sub>2</sub> (wt%)	Al <sub>2</sub> O <sub>3</sub> (wt%)	Fe <sub>2</sub> O <sub>3</sub> (wt%)	FeO (wt%)	MgO (wt%)	CaO (wt%)	Na <sub>2</sub> O (wt%)	K <sub>2</sub> O (wt%)	MnO (wt%)	TiO <sub>2</sub> (wt%)	P <sub>2</sub> O <sub>5</sub> (wt%)	Sr (μg g <sup>-1</sup> )	Rb (μg g <sup>-1</sup> )	Ba (μg g <sup>-1</sup> )	Zr (μg g <sup>-1</sup> )	CIA <sup>a</sup>	LOI (%)
PB																		
B	0.20	39.47	26.32	13.10	1.39	0.78	0.12	0.11	1.33	0.03	1.38	0.13	54.20	83.00	193.00	281.00	94.20	16.69
	0.30	29.52	31.60	16.21	0.93	0.83	0.13	0.10	1.39	0.05	1.18	0.13	54.90	82.30	163.00	226.00	95.00	18.77
	0.40	29.58	31.54	16.09	0.74	0.85	0.16	0.11	1.40	0.04	1.17	0.13	54.50	80.90	163.00	227.00	94.90	18.79
	0.50	29.65	31.91	16.08	0.57	0.88	0.17	0.10	1.43	0.05	1.16	0.13	55.40	84.30	160.00	225.00	94.90	18.29
	0.60	29.89	32.17	16.18	0.64	0.86	0.10	0.10	1.36	0.04	1.14	0.13	52.40	80.50	157.00	220.00	95.10	17.95
	0.70	30.07	32.05	16.13	0.51	0.87	0.08	0.10	1.41	0.05	1.14	0.13	52.90	83.80	155.00	217.00	95.00	17.88
	0.80	29.66	32.30	16.23	0.46	0.84	0.09	0.10	1.36	0.04	1.14	0.13	53.30	81.80	158.00	221.00	95.20	17.99
	0.90	29.33	32.27	16.47	0.41	0.86	0.09	0.11	1.36	0.05	1.14	0.15	51.50	80.80	153.00	215.00	95.10	17.90
	1.00	30.10	32.17	15.97	0.41	0.89	0.07	0.11	1.59	0.07	1.21	0.16	52.90	89.40	169.00	224.00	94.40	17.58
	1.10	30.95	31.78	15.69	0.51	0.97	0.07	0.11	1.74	0.07	1.23	0.16	52.10	91.90	171.00	226.00	93.90	17.21
	1.20	30.68	31.64	15.60	0.45	0.93	0.07	0.11	1.54	0.06	1.17	0.16	51.90	88.40	167.00	209.00	94.50	17.45
	1.30	30.61	31.66	15.96	0.50	0.92	0.07	0.11	1.40	0.06	1.14	0.17	45.90	69.80	149.00	208.00	94.90	17.64
	1.40	30.95	31.90	15.71	0.28	0.95	0.07	0.11	1.49	0.09	1.13	0.17	51.40	93.40	161.00	208.00	94.70	17.36
	1.50	30.94	31.83	15.48	0.33	0.94	0.08	0.11	1.47	0.11	1.15	0.18	52.00	89.00	175.00	210.00	94.70	17.58
	1.60	31.62	31.43	15.22	0.34	0.92	0.08	0.11	1.43	0.12	1.21	0.18	52.50	88.50	184.00	214.00	94.80	17.45
	1.70	31.74	31.08	14.90	0.24	1.11	0.13	0.11	1.99	0.32	1.25	0.18	52.00	105.00	200.00	226.00	93.00	17.09
	1.80	31.90	30.86	14.89	0.25	1.10	0.10	0.12	2.02	0.31	1.25	0.18	52.30	108.00	205.00	229.00	92.80	17.12
C1	1.90	0.86	0.53	0.14	0.12	20.98	30.81	0.03	0.13	0.01	0.04	0.01	74.00	3.85	8.23	7.24	70.10	45.93
C2	2.00	0.80	0.45	0.11	<0.10	20.86	30.84	0.04	0.13	0.01	0.03	0.01	76.70	3.43	7.18	6.65	63.60	46.14
C3	nd	0.49	0.28	0.14	<0.10	20.27	31.74	0.04	0.08	0.01	0.03	0.01	67.90	2.20	5.39	4.08	57.90	46.41
HZB																		
A	0.00	45.64	19.44	12.12	4.84	0.85	1.65	0.13	1.06	0.10	1.67	0.15	46.53	98.00	197.94	267.72	92.50	17.03
	0.10	46.19	21.36	13.01	2.61	0.79	0.74	0.12	1.07	0.10	1.79	0.12	42.29	105.83	197.79	270.99	93.20	14.64
	0.20	47.33	21.54	12.66	1.34	0.77	0.64	0.11	1.08	0.11	1.85	0.11	41.52	107.86	211.58	291.93	93.40	13.77
	0.30	47.35	20.99	13.18	1.97	0.73	0.61	0.10	1.04	0.10	1.79	0.11	41.10	104.29	205.63	289.09	93.50	13.84
	0.40	49.16	20.32	12.59	1.67	0.71	0.59	0.11	1.07	0.12	1.85	0.10	40.77	104.77	207.53	292.71	93.10	13.27
	0.50	54.67	17.90	11.06	0.64	0.67	0.52	0.11	1.07	0.14	2.00	0.09	44.04	102.17	215.91	326.80	92.10	11.47

Table 2 continued

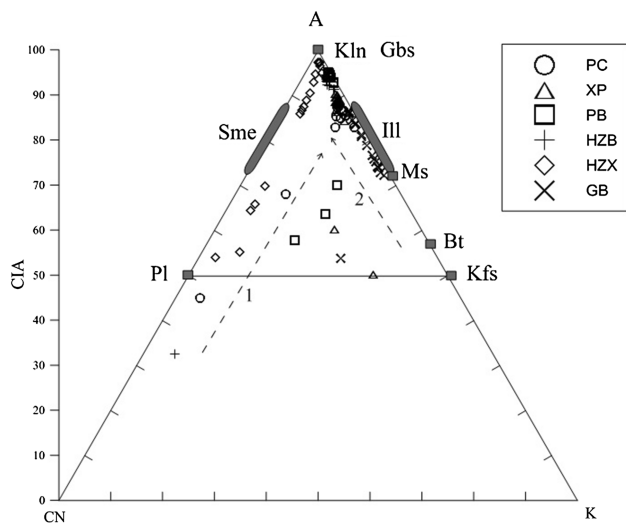
Horizon	Depth (m)	SiO <sub>2</sub> (wt%)	Al <sub>2</sub> O <sub>3</sub> (wt%)	Fe <sub>2</sub> O <sub>3</sub> (wt%)	FeO (wt%)	MgO (wt%)	CaO (wt%)	Na <sub>2</sub> O (wt%)	K <sub>2</sub> O (wt%)	MnO (wt%)	TiO <sub>2</sub> (wt%)	P <sub>2</sub> O <sub>5</sub> (wt%)	Sr (μg g <sup>-1</sup> )	Rb (μg g <sup>-1</sup> )	Ba (μg g <sup>-1</sup> )	Zr (μg g <sup>-1</sup> )	CIA <sup>a</sup>	LOI (%)	
B	0.60	49.82	19.49	13.71	0.50	0.63	0.72	0.09	0.93	0.10	1.87	0.08	39.71	88.09	144.38	253.39	93.70	12.43	
	0.80	45.66	21.98	13.89	0.60	0.72	0.71	0.11	1.06	0.11	1.97	0.09	40.59	103.58	167.48	264.40	93.50	13.52	
	1.00	40.01	24.94	14.71	0.68	0.81	0.67	0.11	1.13	0.09	1.80	0.09	38.27	119.16	204.47	258.49	94.10	15.41	
	1.20	36.48	26.56	15.52	0.66	0.87	0.67	0.10	1.18	0.09	1.65	0.09	36.03	123.75	212.00	243.20	94.30	16.58	
	1.40	36.08	26.84	15.05	1.00	0.88	0.72	0.12	1.08	0.08	1.52	0.11	33.30	117.52	209.56	227.48	94.50	17.47	
	1.60	39.44	25.17	14.38	0.91	0.86	0.78	0.10	1.06	0.11	1.68	0.09	38.19	111.85	214.91	256.32	94.40	16.14	
	1.80	36.82	26.38	13.93	1.33	1.12	0.99	0.11	1.98	0.07	1.58	0.10	37.70	134.59	250.72	243.90	91.30	16.67	
	2.00	40.28	25.21	12.89	0.48	1.04	0.93	0.12	1.85	0.07	1.70	0.10	40.47	139.58	257.01	258.96	91.30	15.58	
	2.20	37.00	25.75	14.10	0.53	0.93	0.39	0.13	1.19	0.08	1.54	0.13	40.54	120.73	219.71	229.10	93.80	17.51	
	C3	nd	0.40	0.08	0.07	<0.10	2.11	54.12	0.04	0.01	0.00	0.00	0.00	258.37	0.33	2.36	1.82	32.50	42.55
HZX	A	0.00	41.70	15.66	17.92	3.28	1.98	2.04	0.53	0.59	0.19	5.32	0.33	142.00	23.19	521.23	438.72	86.70	13.63
	0.05	41.64	16.08	18.02	2.36	1.72	1.34	0.34	0.50	0.19	5.41	0.29	124.05	22.95	496.39	436.18	90.60	14.36	
	0.15	41.25	15.27	19.02	2.31	2.00	1.67	0.40	0.51	0.20	5.71	0.31	139.89	22.22	479.93	463.62	89.00	13.59	
	0.25	42.14	15.65	18.08	2.39	1.96	1.94	0.49	0.57	0.19	5.39	0.31	154.28	24.88	488.73	438.36	87.60	13.27	
	0.35	43.02	15.61	17.63	2.66	2.09	2.29	0.59	0.59	0.19	5.24	0.32	200.00	22.73	484.70	418.06	85.90	12.37	
	B	0.45	41.79	15.90	18.58	1.90	1.48	0.86	0.23	0.42	0.19	5.60	0.24	91.88	23.23	397.36	462.60	93.00	14.62
	0.65	40.34	16.90	19.38	1.13	1.02	0.21	0.09	0.28	0.18	5.96	0.24	37.35	19.64	384.50	478.02	97.40	15.28	
	0.85	38.60	17.87	19.59	1.09	1.44	0.34	0.14	0.26	0.19	5.60	0.29	49.24	17.23	607.97	463.22	97.20	15.61	
	1.05	38.21	18.21	19.09	1.17	1.82	0.69	0.19	0.36	0.20	5.33	0.35	76.35	15.48	862.55	451.90	94.80	15.50	
	1.25	38.42	18.25	18.87	0.76	1.76	0.41	0.10	0.23	0.15	5.13	0.28	54.98	13.69	609.30	431.64	97.30	16.36	
	1.45	40.77	15.68	19.69	0.69	1.72	0.33	0.13	0.30	0.21	5.89	0.25	58.12	15.79	561.61	445.65	96.70	14.97	
C2	1.55	38.51	16.53	18.81	0.29	2.24	0.57	0.20	0.51	0.14	5.75	0.43	85.18	15.17	1,058.70	472.07	95.00	16.13	
	2.15	46.02	13.28	14.73	3.98	3.81	8.46	1.46	0.85	0.15	4.33	0.50	538.75	15.18	492.64	357.45	69.90	6.28	
	2.85	47.66	13.27	14.59	0.37	4.00	8.56	1.79	0.91	0.20	4.23	0.51	549.74	14.28	525.74	340.58	65.90	4.00	
	3.55	48.29	13.27	14.40	6.46	4.10	8.62	1.93	0.91	0.18	4.19	0.48	635.08	13.39	477.80	344.85	64.40	3.47	
	4.25	47.86	13.11	14.67	5.89	4.00	6.48	3.15	0.70	0.16	4.22	0.50	512.21	16.04	444.70	353.02	54.10	4.99	
	C3	nd	49.29	12.41	14.72	8.32	4.04	7.19	2.56	1.49	0.19	4.31	0.51	542.73	38.03	433.66	382.72	55.30	3.10
GB	A	0.00	64.95	15.25	3.06	2.21	0.32	0.06	0.11	2.11	0.02	0.28	0.08	11.35	182.89	60.39	104.69	86.00	13.80
	0.10	65.26	17.09	3.40	0.91	0.34	0.06	0.10	2.31	0.02	0.32	0.07	13.39	208.25	70.26	127.33	86.50	10.81	
	0.20	66.15	17.35	3.46	0.81	0.35	0.06	0.11	2.32	0.02	0.33	0.07	13.56	213.58	69.64	133.14	86.50	9.65	
	0.30	65.95	17.47	3.45	0.77	0.36	0.06	0.11	2.37	0.03	0.32	0.07	13.67	206.98	72.74	127.83	86.40	9.68	

Table 2 continued

Horizon	Depth (m)	SiO <sub>2</sub> (wt%)	Al <sub>2</sub> O <sub>3</sub> (wt%)	Fe <sub>2</sub> O <sub>3</sub> (wt%)	FeO (wt%)	MgO (wt%)	CaO (wt%)	Na <sub>2</sub> O (wt%)	K <sub>2</sub> O (wt%)	MnO (wt%)	TiO <sub>2</sub> (wt%)	P <sub>2</sub> O <sub>5</sub> (wt%)	Sr (ug g <sup>-1</sup> )	Rb (ug g <sup>-1</sup> )	Ba (ug g <sup>-1</sup> )	Zr (ug g <sup>-1</sup> )	CIA <sup>a</sup>	LOI (%)
B	0.40	68.66	16.21	3.35	0.85	0.38	0.07	0.10	2.25	0.03	0.32	0.06	13.36	205.69	69.37	129.47	86.10	8.40
	0.50	73.54	14.21	2.87	0.52	0.38	0.06	0.10	2.24	0.03	0.24	0.05	9.68	204.59	49.44	105.07	84.50	6.21
	0.60	70.92	15.52	3.05	0.75	0.39	0.06	0.12	2.64	0.04	0.25	0.05	12.01	230.10	57.64	113.45	83.50	6.88
	0.70	71.06	15.59	2.80	0.51	0.37	0.07	0.14	3.18	0.04	0.22	0.06	12.36	268.34	56.50	103.72	80.90	6.37
	0.80	70.27	15.97	2.97	0.60	0.37	0.06	0.11	2.71	0.04	0.24	0.06	12.08	237.93	59.12	106.35	83.70	7.20
	0.90	69.86	16.13	2.88	0.75	0.37	0.06	0.12	3.23	0.04	0.24	0.06	12.89	275.06	63.00	104.93	81.30	6.95
	1.00	65.53	17.85	3.04	1.03	0.37	0.06	0.13	3.02	0.04	0.27	0.07	14.09	262.55	68.31	98.07	83.70	9.45
	1.10	71.18	15.71	2.28	0.73	0.33	0.06	0.13	3.67	0.04	0.18	0.06	14.35	295.62	54.78	91.58	78.90	6.36
	1.20	71.64	15.30	2.38	0.83	0.34	0.06	0.15	4.26	0.04	0.19	0.06	16.95	330.89	73.27	99.38	75.90	5.55
	1.30	71.43	15.76	2.20	0.70	0.33	0.06	0.15	4.20	0.04	0.17	0.06	15.03	315.59	53.43	93.02	76.70	5.58
C3	1.40	73.41	14.46	2.22	0.84	0.34	0.07	0.17	4.38	0.05	0.18	0.06	18.00	327.04	59.93	109.61	74.20	4.61
	1.50	71.41	15.84	2.04	0.84	0.32	0.06	0.17	4.54	0.04	0.16	0.07	14.64	340.00	69.60	94.89	75.30	5.32
	1.60	69.45	16.71	2.14	1.21	0.34	0.07	0.21	5.41	0.04	0.17	0.08	22.58	398.65	138.27	84.41	72.90	5.38
	1.70	71.77	15.38	2.18	1.25	0.32	0.07	0.17	4.72	0.04	0.18	0.07	19.66	352.34	68.14	88.69	74.00	5.07
	1.80	71.47	15.54	2.28	0.70	0.36	0.06	0.17	4.69	0.05	0.20	0.07	20.20	371.83	65.69	109.60	74.40	5.09
nd	1.90	71.38	15.32	2.30	0.63	0.43	0.05	0.15	5.20	0.04	0.18	0.05	14.74	423.72	72.37	93.63	72.20	4.91
	2.00	76.18	12.70	1.51	1.11	0.18	0.51	2.27	5.96	0.03	0.10	0.12	17.90	314.96	20.27	72.79	53.90	0.45

<sup>a</sup> not determined

<sup>a</sup> Chemical index of alteration (CIA) = Al<sub>2</sub>O<sub>3</sub>/(Al<sub>2</sub>O<sub>3</sub> + CaO\* + Na<sub>2</sub>O + K<sub>2</sub>O), where CaO\* represents the Ca in silicate (calculated according to reference of Fedo et al. 1995; McLennan 1993)



**Fig. 2** Ternary diagram of molecular proportions  $\text{Al}_2\text{O}_3$ – $\text{CaO}^*$  +  $\text{Na}_2\text{O}$ – $\text{K}_2\text{O}$ . Plotted are estimates of all samples of each site in this study, including unweathered bedrocks, weathered rocks, regolith and soil. Also plotted is the idealized mineral compositions. Dotted line represent the weathering trend (weathering trend 1 and 2). Shown at the left side is the CIA scale. *Kln* kaolinite, *Gbs* gibbsite, *Ill* illite, *Ms* muscovite, *Bt* biotite, *Kfs* K-feldspar, *Pl* plagioclase, *Sme* smectite

and Na and accumulating Al, weathering trend 2 represents the process of leaching K and accumulating Al. For the carbonate profiles (PC, HZB, XP, PB), most samples of the regolith can't be notably distinguished and almost flock together close to the area between where the illite lies and the A end. The PC, PB and HZB first experience weathering trend 1 and then trend 2. In weathering trend 1, the Ca and Na are almost completely leached from the C horizon to the B horizon. Weathering trend 2 is not very apparent, the samples of PC are close to the area where the illite lies, and those of PB and HZB tend to approach to the A end. The XP profile experiences the weathering trend 2 from the C3 horizon to the C2 horizon, and then experiences the weathering trend 1 to the joint A–K. The samples of XP lie in the area between where the illite lies and the A end. For the silicate profiles, the GB site first experiences the weathering trend 1 from the C3 horizon to the C2 horizon, and then experiences a clearly distinguishable weathering trend 2. The samples distribute uniformly close along the A–K side, and occupy the area where the illite and muscovite lies. The HZX profile only experiences weathering trend 1, and the samples distribute closely along the A–CN side, which demonstrate a wide range of weathering intensity, from unweathered to slightly weathered, to intensely weathered and finally, near the composition of pure aluminosilicate minerals.

The mineral composition is purer for carbonate rocks than for silicate rocks (Table 3). The difference is caused by different analyzing methods and the natural properties of the rock itself. The carbonate rocks are composed of

Site	Quartz	Albite	Calcite	Dolomite	Anorthite	Orthoclase	Cordundum wt%	Diopside	Hypersilene	Ilmenite	Magnetite	Apatite	Zircon
PC	5.66	1.21	93.13										
XP	1.82			98.18									
PB			1.86	98.14									
HZB			93.76	6.24									
HZX	5.74	20.74			17.21	8.43		11.69	15.79	7.84	11.38	1.12	0.08
GB	38.55	19.08			1.75	34.99	1.86		1.16	0.19	2.15	0.26	0.01

**Table 3** Minerals of the protolith of each site

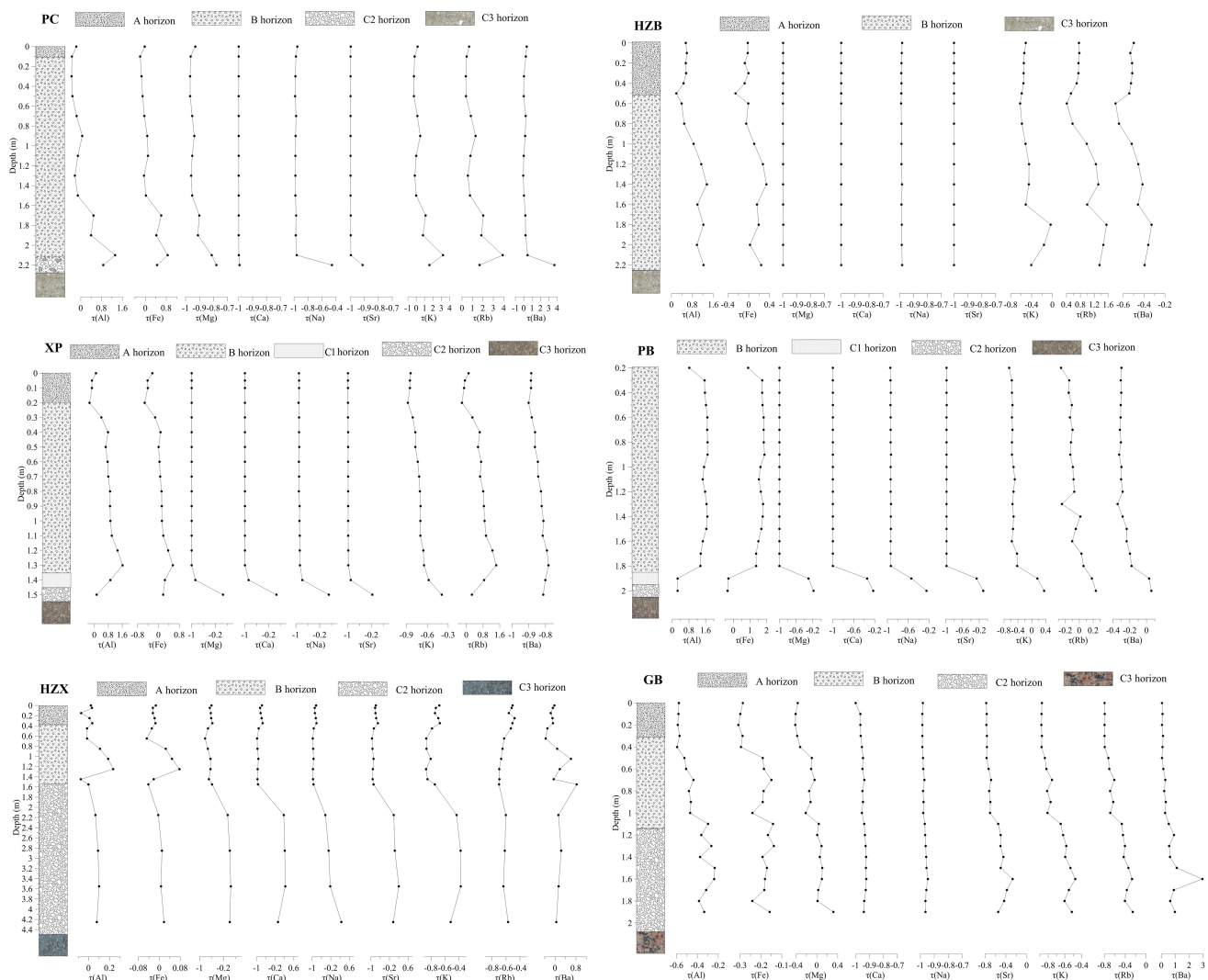


**Fig. 3** Elemental mobilities at each profiles.  $\tau_j$  is the mass transfer coefficient from Eq. (1)

nearly pure calcite or dolomite. The mineral composition of silicate rocks is complex. For HZX (basalt), its main minerals include feldspar, pyroxene and iron oxides. The parent rock at the GB site (granite) is composed mainly by quartz, albite and orthoclase (Table 3).

## 4 Discussion

### 4.1 Weathering process of carbonate and silicate rocks

As shown in the A–CN–K diagram (Fig. 2), the weathering process of carbonate profiles (PC, HZB, XP, PB) can be divided into two stages. The weathering reaction mainly happens at the first stage in the C horizon (including C1, C2 and C3), with the almost completely leaching of Ca and Na and the accumulation of Al. The second stage is the further weathering of insoluble residua, which is similar to the weathering of the

GB profile, with the leaching of K and accumulation of Al. At the silicate profiles (HZX and GB), weathering happens more gradually throughout the whole profile, than at the carbonate profiles. The difference comes from the different protolith compositions. The main minerals in carbonate rocks are calcite or dolomite (Table 3). The high solubility of calcite and dolomite allow them to be easily leached out at the initial stage, especially in a climate with high precipitation (Table 1). The main minerals in silicate rocks in this study are quartz, feldspar and pyroxene; their weathering resistances are stronger than calcite and dolomite's, so, weathering reactions take place more gradually along the whole profiles.

### 4.2 Elemental mobility

The weathering intensity can be described by comparing the element concentrations of the regolith to those of the original protolith ( $\frac{C_{jw}}{C_{jp}}$ ). This ratio is affected by the gains

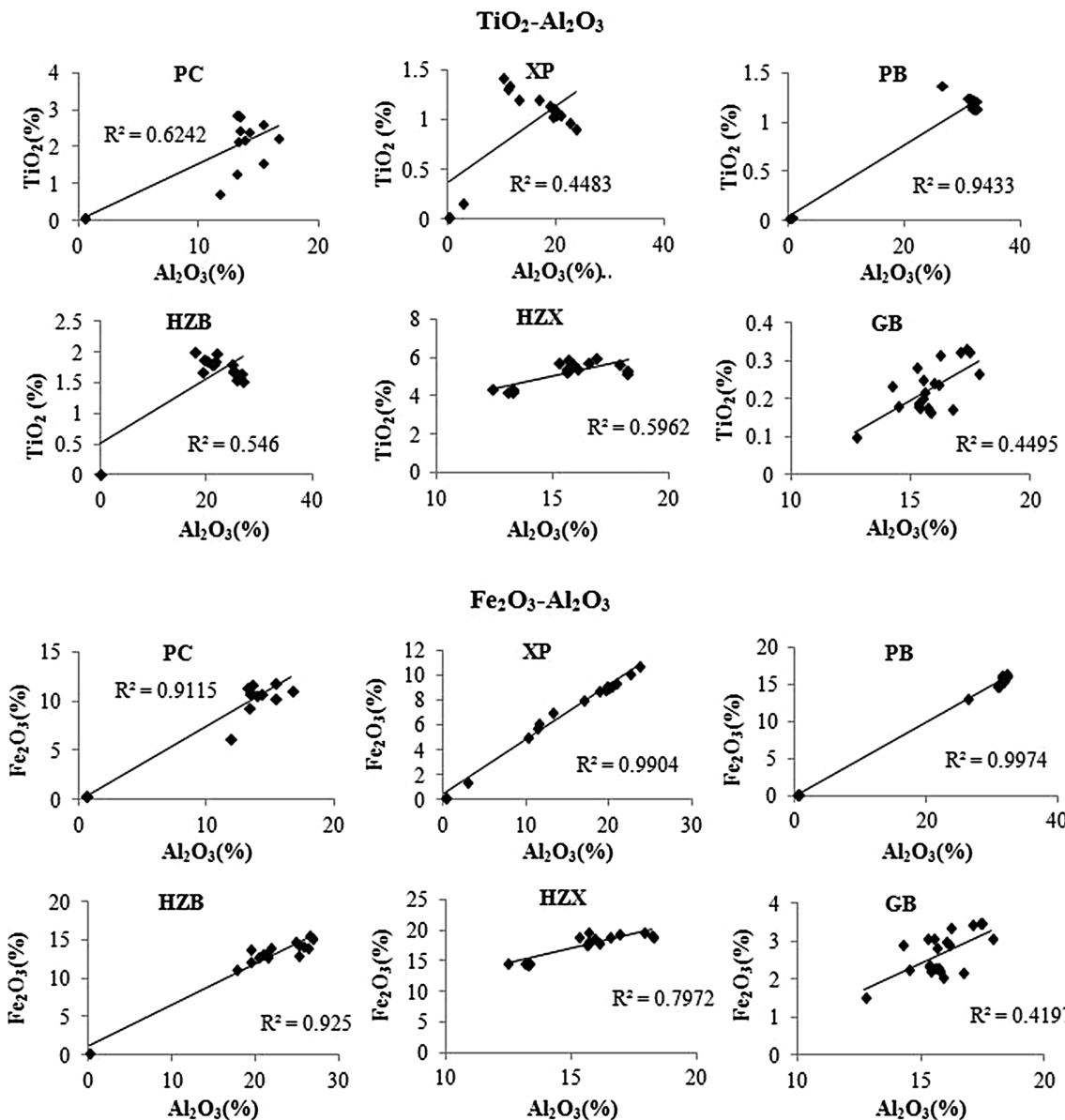


**Fig. 4** Relationships between Al<sub>2</sub>O<sub>3</sub> and TiO<sub>2</sub>, Al<sub>2</sub>O<sub>3</sub> and Fe<sub>2</sub>O<sub>3</sub> in soil profiles

and losses of other components and the compaction or dilation of the regolith. Solving such a problem requires comparing the ratio of the mobile component, *j*, to the ratio of an additional inert component, *i*.

$$\tau_j = \frac{C_{jw} \cdot C_{ip}}{C_{jp} \cdot C_{iw}} - 1 \quad (1)$$

$\tau_j$  is the mass transfer coefficient (Brimhall and Dietrich, 1987). The value of  $\tau_j = 0$  denotes no mobility,  $\tau_j = -1$  indicates complete leaching out and  $\tau_j > 0$  denotes external additions. Refractory elements such as Zr, Ti and Nb are commonly used as conservative components, *C<sub>i</sub>*, in Eq. (1) (Brimhall et al. 1991; Merritts et al. 1991; White et al. 1998; Riebe et al. 2001). In this study, we use Ti as the

inert component. The original protolith component is that of the sample in the C horizon for each site.

For carbonate rocks (PC, HZB, XP, PB), the main minerals are calcite and dolomite (Table 3); the weathering intensity of calcite is reflected in the mobility of Ca and the weathering intensity of dolomite is reflected in mobility of Ca and Mg. For silicate rocks, the minerals are more complex: the weathering intensity of plagioclase is reflected in the mobility of Na, Ca and Sr and the weathering intensity of K-feldspar is reflected in the mobility of K, Rb and Ba. Al, Fe and Mg concentrations reflect the weathering of smectite and the formation of secondary kaolinite, gibbsite and Fe oxides (White et al. 2008).

As shown in Fig. 3, in the profiles developed on carbonate rocks (PC, HZB, XP, PB), the Mg, Ca, Na and Sr are totally lost in the B and A horizons. The Sr can replace Ca and, when contained in calcite, the similar  $\tau_j$  depth distribution of Mg, Ca and Sr demonstrates carbonate and dolomite weathering. The Na mobility has a similar depth change as that of Mg, Ca and Sr because of its mobile character in carbonate weathering. The higher  $\tau_j$  of Na that appears at the C2 horizon of the PC profile demonstrates the slower weathering rate of the albite composed in the bedrock (Table 3). The higher  $\tau_j$  of Mg, Ca, Na and Sr in the C horizon of the XP and PB than that of the PC and HZB is caused by the slower dissolution rate of dolomite compared to the dissolution rate of calcite.

At the profiles developed on the silicate rocks, the weathering process of basalt (HZX) is different from that of granite (GB). At HZX, the element mobility barely changes at the C2 horizon, with the largest variation happening at the C2-B (rock-regolith) interface. The Mg, Ca, Na and Sr are greatly depleted at the interface and are then almost unchanged in the B and A horizon, reflecting the weathering of the feldspar and pyroxene that mainly occurred at the C2-B interface. At the GB site, Ca and Na are almost completely lost, reflecting the intense weathering of albite and anorthite. The Al, Fe and Mg mobility change synchronously, reflecting the weathering of muscovite and illite. The gradually decreasing  $\tau_j$  of K and Ba reflects the weathering of K-feldspar. The decreased mobility of K, Ba and Rb relative to Na and Ca reflect the slower weathering of K-feldspar relative to plagioclase (Nesbitt and Young, 1984; White et al. 2001).

At both the carbonate and silicate profiles, the Al and Fe mobility change synchronously, reflecting their similar geochemistry behavior in the study profiles. Except for the GB profile, Fe and Al accumulation is accompanied by the loss of mobile elements. The fact that Fe is not accumulated relative to protolith in the GB profile may result from the lack of clay in the environment, which is in favor of the formation of iron oxides in comparison to other profiles. The less clay in the GB is reflected in the lower LOI (Table 2). The extremely high amount of precipitation at the GB site (Table 1) may also contribute to the leaching of the Fe.

#### 4.3 Determining the sink of CO<sub>2</sub> based on elemental weathering gradients in regolith

In studies on CO<sub>2</sub> consumption by chemical weathering, one method is to use the solid-state elemental changes between protolith and regolith. However, the allochthonous components carried by wind or water present a limit for the application of the mass balance approach when calculating CO<sub>2</sub> consumption (Schellmann 1989; Maynard 1992). It's important to determine whether the allochthonous components have affected the component in the profile. The elements Al, Ti and Fe are the less mobile elements, and there is a positive

correlation between Al<sub>2</sub>O<sub>3</sub> and TiO<sub>2</sub>, as well as Al<sub>2</sub>O<sub>3</sub> and Fe<sub>2</sub>O<sub>3</sub> (Fig. 4), reflecting the characteristics of the in situ weathering (Young and Nesbitt, 1998). The synchronous  $\tau_j$  changes of the element groups (Al–Fe, Al–Fe–Mg and Mg–Ca–Na–Sr) discussed in Sect. 4.2 also demonstrate the in situ weathering of the study profiles. The in situ weathering of the carbonate profiles in the Guizhou province is also demonstrated in detail in other papers (Ji et al. 2004a, b; Feng et al. 2009). So, mass changes can be calculated directly from the differences between elemental compositions in the initial protolith and the weathered regolith.

In the simplest scenario for steady-state weathering, a mobile element, which is not incorporated into secondary precipitates, linearly decreases with decreasing depth from an initial concentration  $C_0$  at depth  $z_1$  to a concentration  $C_w$  at a shallower depth  $z_0$  (Fig. 5) (White, 2002). The elemental concentrations are commonly reported as mol kg<sup>-1</sup>. In order to make direct comparisons of element mobility due to weathering, element change  $\Delta m$  (mol m<sup>-3</sup>) is defined in terms of a unit volume (White, 2002) such that

$$\Delta m = 1000 \rho_w (C_w - C_0) \quad (2)$$

where  $\rho_w$  is the regolith bulk density (g cm<sup>-3</sup>),  $C_0$  (mol kg<sup>-1</sup>) is the initial elemental concentration shown in Fig. 5, which is assumed to be that of the protolith, and  $C_w$  (mol kg<sup>-1</sup>) is the elemental concentration at the weathered regolith. Under closed system conditions, the difference in concentrations,  $C_0 - C_w$ , reflects the total mass change occurring over the entire time of pedogenesis. The concentration  $C_w$  can't be determined directly from the

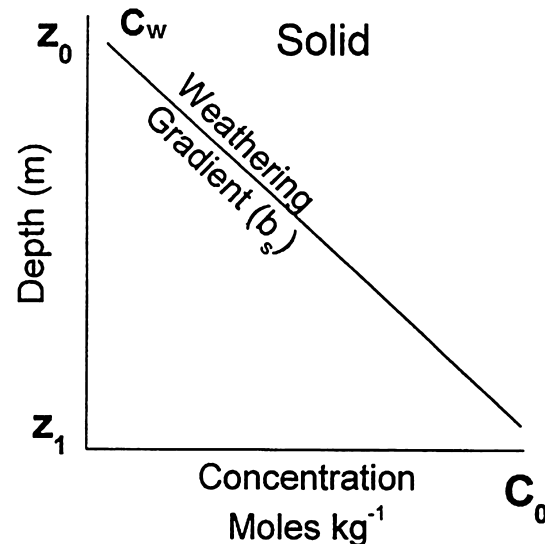


**Fig. 5** Schematic showing the distributions of a mobile element in a weathering regolith.  $C_w$  defines the weathered concentration at shallow depth  $z_0$ , and  $C_0$  is the initial protolith concentration at depth  $z_1$ . The weathering gradients  $b_s$  describe the slope of the linear gradients

measured elemental concentration  $C$ , because  $C$  is also affected by the gains and losses of the other components and the compaction or dilation of the regolith. The element Ti is chosen as the inert component again. The normalized weathering concentration  $C_w$ , is obtained from the measured concentration  $C$  by the relationship

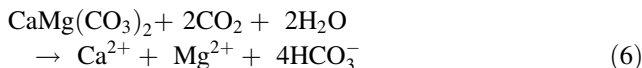
$$C_w = C_0 \left( \frac{I_0}{I_w} \right) \quad (3)$$

where  $I_0$  ( $\text{mol kg}^{-1}$ ) is the concentration of the inert element in the protolith and  $I_w$  is the concentration in the weathered regolith (White, 2002). The slope of the gradient in Fig. 5 is defined as  $b_s$  ( $\text{m kg mol}^{-1}$ ). Therefore,  $C_w - C_0 = \Delta z/b_s$ . Substituting this relationship into Eq. (2) results in the expression

$$\Delta m = 1000 \rho_w \left( \frac{\Delta z}{b_s} \right) \quad (4)$$

As discussed in Sect. 4.2, the Mg, Ca, Na, K is the main mobile element in most minerals of the carbonate and silicate rocks, and their concentration change will reflect the chemical weathering intensity, thus reflecting the drawdown of atmospheric  $\text{CO}_2$ . In this study, we ignore the role of organic acid and sulfuric acid that may take part in the chemical weathering, and regard the  $\text{CO}_2$  as the only acid source that participates in the weathering reaction.

The weathering reaction that happened at the carbonate profiles at the initial stage were mainly the leaching of calcite and dolomite demonstrated in the following equations:



The further weathering reactions of the residues on carbonate rocks are mainly the reactions of non-carbonate minerals.

The main chemical weathering reactions that happened at the silicate profiles based on their main minerals are

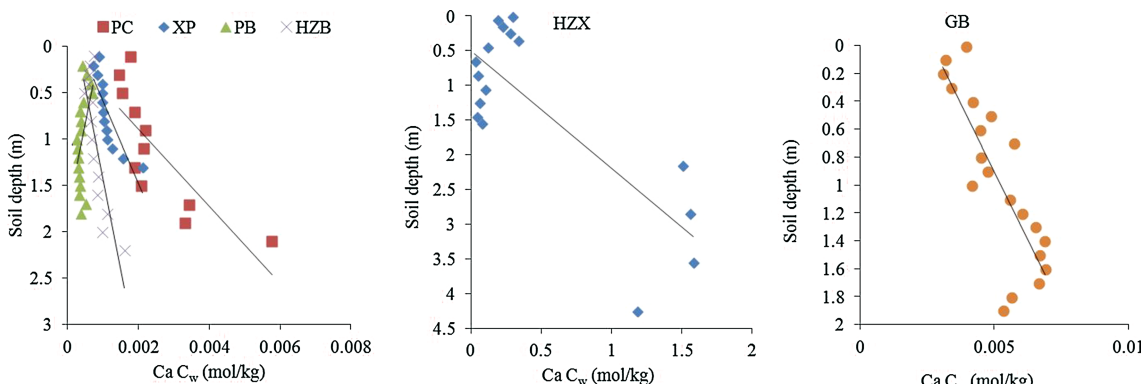
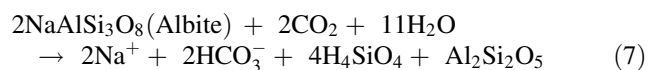
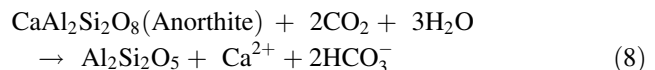


**Fig. 6** Normalized concentrations of Ca ( $C_w$ ) plotted as a function of depth in regolith. The lines are the linear regression fits describing the weathering gradients  $b_s$

mainly the weathering of albite, anorthite, orthoclase and pyroxene as follows



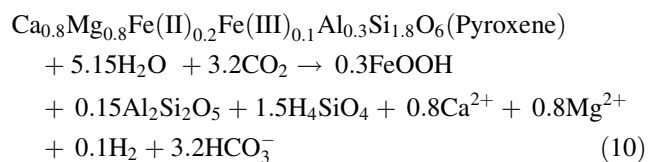
(Suchet and Probst 1995)



(Garrels and Mackenzie 1971)



(Huh 2003)



(Sak et al. 2004)

From Eq. (5) to (10), it can be seen that no matter what chemical reaction happened, for carbonate minerals, two mole of base cation charge consume 1 mol of  $\text{CO}_2$ . For non-carbonate minerals, one mole of base cation charge consumes 1 mol of  $\text{CO}_2$ . The  $\text{CO}_2$  captured per volume  $M(\text{CO}_2)$  ( $\text{mol cm}^{-3}$ ) by carbonate and non-carbonate mineral weathering is defined as

$$M(\text{CO}_2)_{\text{carbonate}} = \Delta m(\text{Ca}) + \Delta m(\text{Mg}) \quad (11)$$

$$\begin{aligned} M(\text{CO}_2)_{\text{non-carbonate}} = 2\Delta m(\text{Ca}) + 2\Delta m(\text{Mg}) + \Delta m(\text{Na}) \\ + \Delta m(\text{K}) \end{aligned} \quad (12)$$

There is a certain deviation in the calculation of  $M(\text{CO}_2)$  based on the elemental change, because  $\text{CO}_2$  isn't the only acid source that participates in the weathering reaction. Also, not all elements that reacted with  $\text{CO}_2$  in the profiles are included. Nevertheless, the results can be used to

compare the different capabilities of capturing  $\text{CO}_2$  between the carbonate and silicate profiles in the study area.

#### 4.3.1 Calculation of $\text{CO}_2$ captured per volume of regolith $M_{\text{regolith}}(\text{CO}_2)$

The normalized weathering concentration,  $C_w$ , of Ca, Na, K, and Mg are plotted as functions of depth in Figs. 6, 7, 8,

and 9 respectively. The points plotted for PC, XP, PB and HZB are confined in the B and A horizons. The HZX and GB are confined in C2, B and A horizons. The linear regression equations and the correlation coefficient ( $R^2$ ) drawn from Figs. 6, 7, 8, and 9 are tabulated in Table 4. At the PB site, the Ca increases slightly in the shallower soils (Fig. 6), which results in negative gradients (Table 4). Such an increase may be attributed to the upward biologic

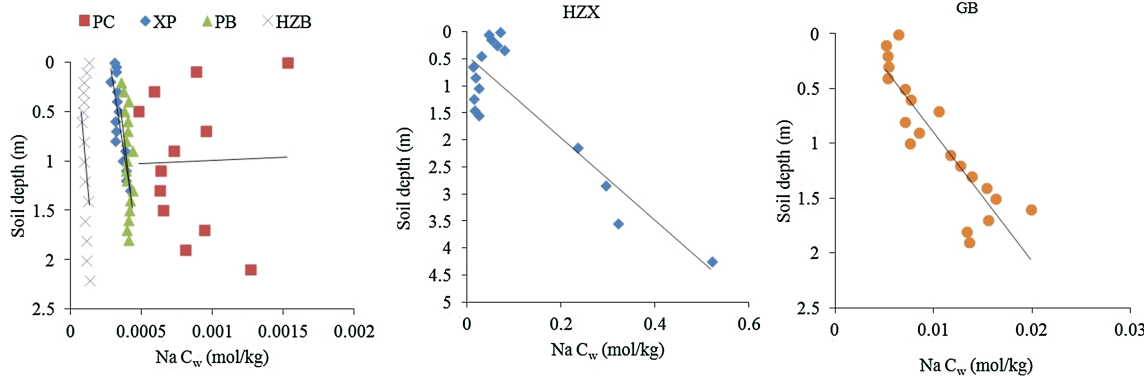


**Fig. 7** Normalized concentrations of Na ( $C_w$ ) plotted as a function of depth in regolith. The lines are the linear regression fits describing the weathering gradients  $b_s$

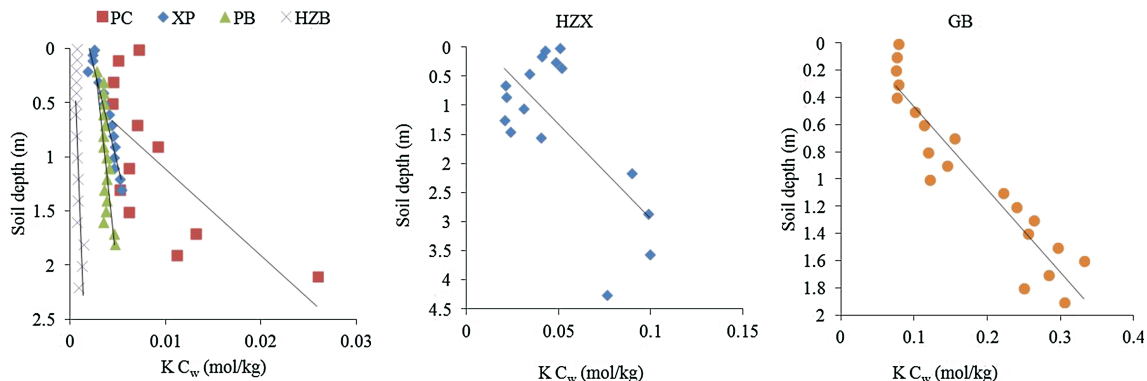


**Fig. 8** Normalized concentrations of K ( $C_w$ ) plotted as a function of depth in regolith. The lines are the linear regression fits describing the weathering gradients  $b_s$

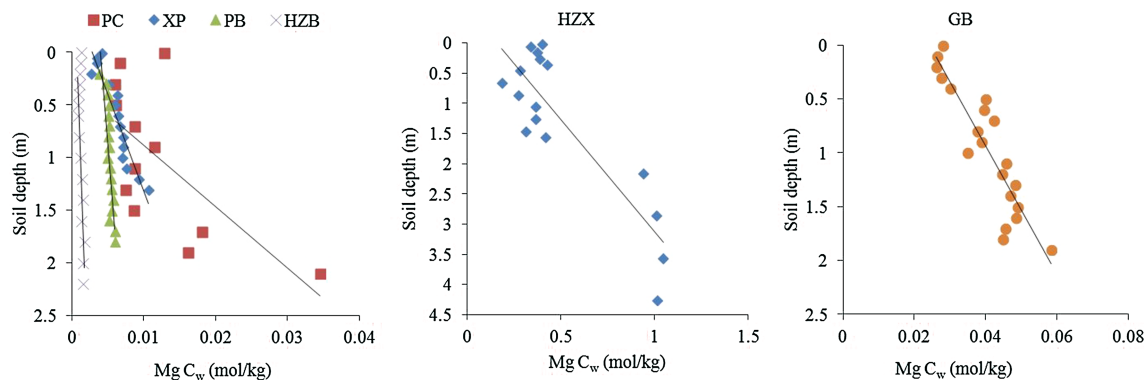


**Fig. 9** Normalized concentrations of Mg ( $C_w$ ) plotted as a function of depth in regolith. The lines are the linear regression fits describing the weathering gradients  $b_s$

**Table 4** The linear regression equations and the correlation coefficient ( $R^2$ ) drew from Figs. 6, 7, 8 and 9

Sampling sites	Number of data (n)	Linear equation	Correlation coefficient ( $R^2$ )	Linear equation	Correlation coefficient ( $R^2$ )	Linear equation	Correlation coefficient ( $R^2$ )	Linear equation	Correlation coefficient ( $R^2$ )
Ca									
PC	12	$y = 416.0x + 0.06$	0.627	$y = -65.2x + 1.06$	0.000	$y = 79.6x + 0.32$	0.463	$y = 58.1x + 0.30$	0.438
XP	15	$y = 885.2x - 0.28$	0.672	$y = 9.155.4x - 2.54$	0.689	$y = 364.3x - 0.74$	0.922	$y = 185.7x - 0.54$	0.870
PB	17	$y = -1,944.7x + 1.78$	0.245	$y = 12773x - 4.08$	0.276	$y = 827x - 2.02$	0.534	$y = 849.8x - 3.37$	0.693
HZB	15	$y = 1,958.7x - 0.54$	0.657	$y = 17252x - 0.83$	0.140	$y = 2233x - 0.69$	0.577	$y = 1,949.6x - 1.38$	0.564
HZX	16	$y = 1.7x + 0.49$	0.616	$y = 7.6x + 0.45$	0.767	$y = 32.4x - 0.30$	0.471	$y = 3.7x - 0.58$	0.751
GB	20	$y = 387.6x - 1.04$	0.674	$y = 117.2x - 0.27$	0.778	$y = 6.1x - 0.14$	0.877	$y = 59.6x - 1.44$	0.811
Na									
K									
Mg									

pumping via plant roots and the subsequent recycling in the shallow soils (White et al. 2009; White 2014). Because the  $C_w$  of Ca in the PB regolith is relatively small in comparison to those in the other sites (Fig. 6), it is acceptable to not use the Ca concentration in the calculation of  $M(\text{CO}_2)$ . The Na didn't show any linear fit to the data at the PC site (Table 4). To clarify the reason for this, the surface soil was analyzed by XRD, and the semiquantitative calculation of the mineral composition shows that the surface soil of the PC was composed of albite (2.82 %), hornblende (1.16 %), quartz (88.35 %), smectite (1.85 %), illite (2.83 %), kaolinite (1.87 %) and iron oxides (1.12 %). Albite and hornblende are primary minerals. Albite appeared in the bedrock of the PC (Table 4). Even so, the presence of it at the surface is likely from the allochthonous materials, as albite is easily weathered at deep depths. Hornblende is not present in the bedrock, demonstrating the deposition of the allochthonous materials. Except for albite and hornblende, the others are secondary minerals, which are usually found in the weathering residues of carbonate rocks (Ji et al. 2004a, b). Primary minerals that are not present in the bedrock also appeared at the surface of the PB [albite (0.52 %) and hornblende (1.30 %)] and HZB sites [albite (1.31 %)]. This may explain the lower linear correlation coefficient for Na at the PC, PB and HZB sites. The  $C_w$  of Na in carbonate regolith is small (about  $0\text{--}0.002 \text{ mol kg}^{-1}$ ) (Fig. 7), and it is about ten orders of magnitudes smaller than that of Ca, K and Mg. Therefore, the effect of the allochthonous materials is neglected and the Na concentrations of the PC, PB and HZB were not included in the calculation of  $M(\text{CO}_2)$ . The  $b_s$  in Eq. (4) is the slope of the linear regression equations and the  $\rho_w$  is the average value of the bulk density of each horizon (Table 5). The  $M_{\text{regolith}}(\text{CO}_2)$  was calculated according to Eq. (12).

The results show that the  $M_{\text{regolith}}(\text{CO}_2)$  of the silicate regolith  $M_{sr}(\text{CO}_2)$  is tens to thousands orders of magnitude greater than that of the carbonate regolith  $M_{cr}(\text{CO}_2)$  (Table 5). This occurs because the elements are greatly leached in the C horizon of the carbonate profiles and the elements that remain in the carbonate regolith are significantly less than that in the silicate regolith. Though the amount of  $\text{CO}_2$  consumed by the insoluble residuals on carbonate rocks is small, it can't be denied that the chemical weathering of them may produce a net sink of  $\text{CO}_2$  in the long-term scale.

For the carbonate profiles, the  $M_{cr}(\text{CO}_2)$  is in the order of  $\text{PC} \gg \text{XP} > \text{PB} \approx \text{HZB}$ . The average CIA value of the carbonate regolith is PC (86), XP (89), PB (94), HZB (93), demonstrating a weathering intensity order of  $\text{PB} \approx \text{HZB} > \text{XP} > \text{PC}$ , which is in the reverse when compared with the order of  $M_{cr}(\text{CO}_2)$ . This is also related to the two-stage weathering process of the carbonate rocks;

**Table 5** The elemental change ( $\Delta m$ ) of Ca, Na, K and Mg and the CO<sub>2</sub> captured per volume of regolith  $M_{regolith}$  (CO<sub>2</sub>)

Sampling sites	$\rho_w$ (g cm <sup>-3</sup> )	$\Delta z$ (m)	$\Delta m_{Ca}$ (mol m <sup>-3</sup> )	$\Delta m_{Na}$ (mol m <sup>-3</sup> )	$\Delta m_K$ (mol m <sup>-3</sup> )	$\Delta m_{Mg}$ (mol m <sup>-3</sup> )	$M$ (CO <sub>2</sub> ) (mol m <sup>-3</sup> )
PC	1.37	2	6.59	–	34.43	47.14	141.89
XP	1.55	1.3	2.28	0.22	5.53	10.85	32.00
PB	1.36	1.8	–	–	2.96	2.88	8.72
HZB	1.4	2.2	1.57	–	1.38	1.58	7.68
HZX	1.48	4.25	3,706.54	828.18	193.84	1,694.50	11,824.10
GB	1.56	1.9	7.65	25.29	488.63	49.74	628.69

**Table 6** The elemental change ( $\Delta m$ ) of Ca and Mg in carbonate rocks and the CO<sub>2</sub> captured per volume of carbonate protolith  $M_{cp}$  (CO<sub>2</sub>)

Sampling sites	$\rho_w$ (g cm <sup>-3</sup> )	$C_{oCa}$ (mol kg <sup>-1</sup> )	$C_{wCa}$ (mol kg <sup>-1</sup> )	$\Delta m_{Ca}$ (mol m <sup>-3</sup> )	$C_{oMg}$ (mol kg <sup>-1</sup> )	$C_{wMg}$ (mol kg <sup>-1</sup> )	$\Delta m_{Mg}$ (mol m <sup>-3</sup> )	$M$ (CO <sub>2</sub> ) (mol m <sup>-3</sup> )
PC	2.69	8.3,791	0.0,058	22,524.3	0.1,833	0.0345	400.3	22,924.6
XP	2.72	5.3620	0.0021	14,578.9	5.2965	0.0106	14,377.5	28,956.4
PB	2.78	5.6598	0.0004	15,733.1	5.0285	0.0059	13,962.9	29,696.1
HZB	2.62	9.6505	0.0016	25,280.1	0.5234	0.0015	1,367.5	26,647.6

higher weathering intensity resulted in less elements left in the carbonate regolith, so the weathering of the regolith would consume less CO<sub>2</sub>. The PC profile belongs to the cambisols in soil classification and weaker development of the profile lead more elements in the regolith. Therefore, the  $M_{cr}$  (CO<sub>2</sub>) of PC is much larger than the other three carbonate profiles. For the silicate profiles, the HZX (CIA = 92) consumes more CO<sub>2</sub> than the GB (CIA = 84), demonstrating that the profile with the higher weathering intensity consumes more CO<sub>2</sub>. This is consistent with the weathering process of silicate.

Usually, warmer and wetter climates yield higher weathering intensity (White 2002; White and Blum 1995), thus possibly leading to a higher carbon sink. The studied profiles were distributed from the west to the east (Fig. 1), with relatively warmer and wetter climates in the east. From Table 1, it can be seen that the mean annual temperature is GB > PB > PC > XP > HZB = HZX and the mean annual precipitation is GB > PB > PC = XP > HZB = HZX, based on the  $M_{regolith}$  (CO<sub>2</sub>) of each site. It seems that there is no correlation between the climate and the  $M_{regolith}$  (CO<sub>2</sub>). However, we cannot conclude that the climate doesn't show any impact on the carbon sink in the study area, because the climatic signals are obscured by the lithologic difference and the pedogenic time.

#### 4.3.2 Calculation of CO<sub>2</sub> captured per volume of carbonate protolith $M_{cp}$ (CO<sub>2</sub>)

The elemental change between the protolith and the regolith in the silicate profiles is small and the weathering

penetrates from the soil horizon to the protolith gradually, so the elemental change calculated based on weathering gradients can reflect the change of the whole silicate profile. However, as discussed in Sects. 4.1 and 4.2, the weathering of the carbonate protolith happened mainly at the rock-regolith interface, with the almost complete loss of Ca and Mg by the reactions of Eq. (5) and Eq. (6). To determine the element change at the interface, the  $C_o$ ,  $C_w$ , and  $\rho_w$  in Eq. (4) are regarded as the elemental concentration of the protolith, and the elemental concentration of the bottom layer of the regolith and the bulk density of the protolith respectively. The CO<sub>2</sub> captured per volume of carbonate rock  $M_{cp}$  (CO<sub>2</sub>) is calculated according to Eq. (11). Based on this principle, the calculated  $M_{cp}$  (CO<sub>2</sub>) are about four times larger than  $M_{sr}$  (CO<sub>2</sub>) (Table 6). The results demonstrate that during the entire time of soil development, the carbonate rocks play a more important role than the silicate rocks in regulating the level of CO<sub>2</sub>.

## 5 Conclusions

This work compared the weathering process of carbonate and silicate rocks and determined the CO<sub>2</sub> captured during this process. Due to the extremely high dissolution rates of calcite and dolomite, the weathering of the carbonate rocks mainly occurred at the rock-regolith interface, with leaching of most mobile element. The further weathering of the insoluble residues on the carbonate rocks is similar to that of granite profile (GB). The silicate weathering, especially the weathering of granite, proceeded more gradually than the carbonate weathering. Therefore, the mass change

occurred at the regolith of the carbonate profiles and the silicate profiles are calculated based on the weathering gradients. The mass change that occurred at the rock-regolith interface of the carbonate profiles was calculated by the elemental differences between the protolith and the bottom regolith layer. The CO<sub>2</sub> consumed by silicate profiles are tens to thousands orders of magnitude greater than that by carbonate regolith. Even so, it demonstrates that the carbonate regolith can be a sink of CO<sub>2</sub> on the long-term scale. The CO<sub>2</sub> consumed by carbonate rocks are about four times larger than that by silicate profiles, implying that carbonate rocks play a more important role than silicate rocks in regulating the level of CO<sub>2</sub> during the pedogenic process of the profiles.

**Acknowledgments** This work was jointly supported by the National Natural Science Foundation of China (NSFC) grants (No. 41073096 and 40473051), National Key Basic Research Program of China (2013CB956702) and the Hundred Talents Program of the Chinese Academy of Sciences. We thank Gong G. H. for the XRD analysis and Hu J. for assistance in the HR-ICP-MS determination.

## References

- Berner RA (1991) A model for atmospheric CO<sub>2</sub> over Phanerozoic time. *Ar J Sci* 291:339–376
- Berner RA (1997) Weathering, plants and long-term carbon cycle. *Geochim Cosmochim Acta* 56:3225–3231
- Berner RA, Lasaga AC, Garrels RM (1983) The carbonate–silicate geochemical cycle and its effect on atmospheric CO<sub>2</sub>. *Am J Sci* 283:641–683
- Brimhall GH, Dietrich WE (1987) Constitutive mass balance relations between chemical-composition, volume, density, porosity, and strain in metasomatic hydrochemical systems—results on weathering and pedogenesis. *Geochim Cosmochim Acta* 51:567–587
- Brimhall GH, Lewis CJ, Ford C, Bratt J, Taylor G, Warin O (1991) Quantitative geochemical approach to pedogenesis-importance of parent material reduction, volumetric expansion, and cation influx in laterization. *Geoderma* 51:51–91
- Fedo CM, Nesbitt HW, Young GM (1995) Unraveling the effects of potassium metasomatism in sedimentary rocks and paleosols, with implications for paleoweathering conditions and provenance. *Geology* 23:921–924
- Feng JL, Cui ZJ, Zhu LP (2009) Origin of terra rossa over dolomite on the Yunnan-Guizhou Plateau, China. *Geochem J* 43:151–166
- Garrels RM, Mackenzie FT (1971) Evolution of sedimentary rocks. Norton and Co. Inc., New York, p 397
- GB/T 14506.14-2010. Silicate rock chemical analytical procedure part 14: determination of ferrous oxide (in Chinese)
- GB/T 14506.28-2010 Silicate rock chemical analytical procedure part 28: determination of 16 primary and secondary components (in Chinese)
- GB/T 50123-1999. Standard for soil test methods part 5: determination of soil density (in Chinese)
- Goudie AS, Viles HA (2012) Weathering and the global carbon cycle: Geomorphological perspectives. *Earth Sci Rev* 113:59–71
- Hartmann J, Jansen N, Dürr HH, Kempe S, Köhler P (2009) Global CO<sub>2</sub>-consumption by chemical weathering: What is the contribution of highly active weathering regions? *Global Planet Change* 69:185–194
- Heckman K, Rasmussen C (2011) Lithologic controls on regolith weathering and mass flux in forested ecosystems of the southwestern USA. *Geoderma* 164:99–111
- Horton TW, Chamberlain CP, Fantle M, Blum JD (1999) Chemical weathering and lithological controls of water chemistry in a high-elevation river systems: Clark's Fork of the Yellowstone River, Wyoming and Montana. *Water Resour Res* 35:1643–1655
- Huh YS (2003) Chemical weathering and climate—a global experiment: a review. *Geosci J* 7:277–288
- Ji HB, Wang SJ, Ouyang ZY, Zhang S, Sun CX, Liu XM, Zhou DQ (2004a) Geochemistry of red residua underlying dolomites in karst terrains of Yunnan-Guizhou Plateau I. The formation of the Pingba profile. *Chem Geol* 203:1–27
- Ji HB, Wang SJ, Ouyang ZY, Zhang S, Sun CX, Liu XM, Zhou DQ (2004b) Geochemistry of red residua underlying dolomites in karst terrains of Yunnan-Guizhou Plateau II. The mobility of rare earth elements during weathering. *Chemical Geology*. 203:29–50
- Kenoyer GJ, Bowser CJ (1992) Groundwater chemical evolution in a sandy silicate aquifer in northern Wisconsin, 2. Reaction modeling. *Water Resour Res* 28:591–600
- Li SL, Liu CQ, Li J, Lang YC, Ding H, Li LB (2010) Geochemistry of dissolved inorganic carbon and carbonate weathering in a small typical karstic catchment of Southwest China: isotopic and chemical constraints. *Chem Geol* 277:301–309
- Macpherson GL, Roberts JA, Blair JM, Townsend MA, Fowle DA, Beisner KR (2008) Increasing shallow groundwater CO<sub>2</sub> and limestone weathering, Konza Prairie, USA. *Geochim Cosmochim Acta* 72:5581–5599
- Maynard JB (1992) Chemistry of modern soils as a guide to interpreting Precambrian paleosols. *J Geol* 100:279–289
- McLennan SM (1993) Weathering and global denudation. *J Geol* 101:295–303
- Merritts DJ, Chadwick OA, Hendricks DM (1991) Rates and processes of soil evolution on uplifted marine terraces, northern California. *Geoderma* 51:241–275
- Moosdorf N, Hartmann J, Lauerwald R, Hagedorn B, Kempe S (2011) Atmospheric CO<sub>2</sub> consumption by chemical weathering in North America. *Geochim Cosmochim Acta* 75:7829–7854
- Moquet J-S, Crave A, Viers J, Seyler P, Armijos E, Bourrel L, Chavarri E, Lagane C, Laraque A, Casimiro WSL, Pombosa R, Noriega L, Vera A, Guyot J-L (2011) Chemical weathering and atmospheric/soil CO<sub>2</sub> uptake in the Andean and Foreland Amazon basins. *Chem Geol* 287:1–26
- Murphy SF, Brantley SL, Blum AE, White AF, Dong HL (1998) Chemical weathering in a tropical watershed, Luquillo mountains, Puerto Rico: II. Rate and mechanism of biotite weathering. *Geochim Cosmochim Acta* 62:227–243
- Nesbitt HW, Young GM (1982) Early proterozoic climates and plate motions inferred from major element chemistry of lutites. *Nature* 299:715–717
- Nesbitt HW, Young GM (1984) Prediction of some weathering trends of plutonic and volcanic-rocks based on thermodynamic and kinetic considerations. *Geochim Cosmochim Acta* 48:1523–1534
- Ridgwell A, Zeebe RE (2005) The role of the global carbonate cycle in the regulation and evolution of the Earth system. *Earth Planet Sci Lett* 234:299–315
- Riebe CS, Kirchner JW, Granger DE, Finkel RC (2001) Strong tectonic and weak climatic control of long-term chemical weathering rates. *Geology* 29:511–514
- Sak PB, Fisher DM, Gardner TW, Murphy K, Brantley SL (2004) Rates of weathering rind formation on Costa Rican basalt. *Geochim Cosmochim Acta* 68:1453–1472
- Schellmann W (1989) Allochthonous surface alteration of Ni-laterites. *Chem Geol* 74:351–364

- Suchet PA, Probst J-L (1995) A global model for present-day atmospheric/soil CO<sub>2</sub> consumption by chemical erosion of continental rocks (GEM-CO<sub>2</sub>). *Tellus B* 47:273–280
- White AF (2002) Determining mineral weathering rates based on solid and solute weathering gradients and velocities: application to biotite weathering in saprolites. *Chem Geol* 190:69–89
- White AF (2014) Chemical weathering of pleistocene glacial outwash sediments: a comparison of contemporary and Long-term rates for soils and groundwaters. *Aquat Geochem* 20:141–165
- White AF, Blum AE (1995) Effects of climate on chemical weathering in watersheds. *Geochim Cosmochim Acta* 59(9):1729–1747
- White AF, Blum AE, Schulz MS, Bullen TD, Harden JW, Peterson ML (1996) Chemical weathering rates of a soil chronosequence on granitic alluvium: 1. Quantification of mineralogical and surface area changes and calculation of primary silicate reaction rates. *Geochim Cosmochim Acta* 60:2533–2550
- White AF, Blum AE, Schulz MS, Vivit DV, Stonestrom DA, Larsen M, Murphy SF, Eberl D (1998) Chemical weathering in a tropical watershed, Luquillo mountains, Puerto Rico: I. Long-term versus short-term weathering fluxes. *Geochim Cosmochim Acta* 62:209–226
- White AF, Bullen TD, Schulz MS, Blum AE, Huntington TG, Peters NE (2001) Differential rates of feldspar weathering in granitic regoliths. *Geochim Cosmochim Acta* 65:847–869
- White AF, Schulz MS, Lowenstern JB, Vivit DV, Bullen TD (2005a) The ubiquitous nature of accessory calcite in granitoid rocks: implications for weathering, solute evolution, and petrogenesis. *Geochim Cosmochim Acta* 69:1455–1471
- White AF, Schulz MS, Vivit DV, Blum AE, Stonestrom DA, Harden JW (2005b) Chemical weathering rates of a soil chronosequence on granitic alluvium: III. Hydrochemical evolution and contemporary solute fluxes and rates. *Geochim Cosmochim Acta* 69:1975–1996
- White AF, Schulz MS, Vivit DV, Blum AE, Stonestrom DA, Anderson SP (2008) Chemical weathering of a marine terrace chronosequence, Santa Cruz, California I: interpreting rates and controls based on soil concentration-depth profiles. *Geochim Cosmochim Acta* 72:36–68
- White AF, Schulz MS, Stonestrom DA, Vivit DV, Fitzpatrick J, Bullen TD, Maher K, Blum AE (2009) Chemical weathering of a marine terrace chronosequence, Santa Cruz, California. Part II: solute profiles, gradients and the comparisons of contemporary and long-term weathering rates. *Geochim Cosmochim Acta* 73:2769–2803
- Young GM, Nesbitt HW (1998) Processes controlling the distribution of Ti and Al in weathering profiles, siliciclastic sediments and sedimentary rocks. *J Sediment Res* 68:448–455
- Zeng C, Gremaud V, Zeng HT, Liu ZH, Goldscheider N (2012) Temperature-driven meltwater production and hydrochemical variations at a glaciated alpine karst aquifer: implication for the atmospheric CO<sub>2</sub> sink under global warming. *Environ Earth Sci* 65:2285–2297